Acta Cryst. (1999). A**55**, 939–954

Refinement of crystal structural parameters using two-dimensional energy-filtered CBED patterns

Kenji Tsuda* and Michiyoshi Tanaka

Research Institute for Scientific Measurements, Tohoku University, Katahira 2-1-1, Aoba-ku, Sendai 980-8577, Japan. E-mail: tsuda@rism.tohoku.ac.jp

(*Received 12 January 1999; accepted 19 April 1999*)

Abstract

A new method to refine crystal structural parameters using convergent-beam electron diffraction (CBED), which is applicable to nanometre-size crystal structure analysis, is proposed. This method is based on the fitting between theoretical calculations and experimental intensities of energy-filtered two-dimensional CBED patterns containing higher-order Laue-zone (HOLZ) reflections. The use of HOLZ reflections is essential for the method because small displacements of atoms can be sensitively detected using HOLZ reflections with large reciprocal vectors. For this purpose, a new Ω-filter transmission microscope (JEM-2010FEF), which can take energy-filtered CBED patterns up to a high angle with a small distortion, and a new analysis program to refine structural parameters, which is based on many-beam Bloch-wave calculations and nonlinear least-squares fitting, have been developed. As a test example, a positional parameter and isotropic and anisotropic Debye–Waller factors of CdS have been refined. Two-dimensional CBED patterns calculated with the refined parameters show very good agreement with the experimental ones, and the refined values of the parameters also agree well with the result of a single-crystal X-ray diffraction experiment. Important problems of the analysis procedure are discussed item by item.

1. Introduction

Crystal structure analysis by the convergent-beam electron diffraction (CBED) method has the following advantages in contrast to the X-ray and neutron diffraction methods:

(i) Nanometre-size crystal structure analysis: CBED patterns can be obtained from specimen areas of a few nanometres in diameter. Therefore, the CBED method enables us to conduct not only the structure determination of perfect crystals but also that of local areas of crystals.

(ii) The dynamical diffraction effect: the CBED intensities contain phase information of crystal structure factors through the strong dynamical effect.

(iii) Site-selective analysis: incident electrons form Bloch states in a specimen also due to the strong dynamical diffraction effect, each Bloch state being concentrated on specific atom positions. The use of the Bloch states allows site-selective structure analysis, or structure determination weighted for specific atom sites. These are characteristic features only for the CBED method.

In recent years, the determinations of crystal structural parameters using the CBED method have been attempted. Vincent *et al.* (1984*a*,*b*) first applied the CBED method to the determination of the atom positions of AuGeAs. They analyzed intensities of higher-order Laue-zone (HOLZ) reflections under the quasi-kinematical approximation. Tanaka & Tsuda (1990, 1991) and Tsuda & Tanaka (1995) refined the structure parameters of the low-temperature phase of $SrTiO_3$ by applying the dynamical theory of electron diffraction for the first time. Rossouw *et al.* (1996) measured the order parameter of TiAl using the Bloch-wave analysis of HOLZ reflections of a CBED pattern. Midgley *et al.* (1996) refined two positional parameters of $AuSn_4$ from diffraction data obtained by a precession technique. Jansen *et al.* (1998) determined atom positions of $La_3Ni_2B_2N_3$, $ThPd_{0.65}B_{4.7}$ and $Ce_5Cu_{19}P_{12}$ from integrated intensities of CBED discs with a small convergence angle using multislice calculations.

We proposed a full dynamical method to refine crystal structure parameters (atom positions and Debye–Waller factors) using CBED patterns with HOLZ reflections for the first time (Tsuda & Tanaka, 1995). The use of HOLZ reflections is essential for the method because small displacements of atoms can be sensitively detected using HOLZ reflections with large reciprocal vectors. The method is based on the least-squares fitting between dynamical calculations and experimental intensities measured by imaging plates. The method was successfully applied to refine the structural parameters of the low-temperature phase of $SrTiO_3$. The experimental intensities in this case were acquired from a thin specimen area without an energy filter. The fitting of the intensities was carried out using both integrated intensities (zero-dimensional data) and one-dimensional line profiles of HOLZ reflections. As already mentioned in

ISSN 0108-7673

the paper of Tsuda & Tanaka (1995), the application of the method without an energy filter requires very thin specimens for reducing inelastic background intensities and suppressing the intensity variation of HOLZ reflections along the azimuthal direction due to dynamical diffraction. The accuracy and reliability of the method can definitely be improved by the use of an energy filter and the two-dimensional data of CBED patterns.

Energy filtering to remove inelastically scattered background is now becoming indispensable for quantitative analysis of CBED patterns. Measurements of low-order structure factors were successfully conducted using energy-filtered CBED patterns by several researchers (Zuo *et al.*, 1989, 1993; Deininger *et al.*, 1994; Saunders *et al.*, 1995, 1996; Cheng *et al.*, 1996; Swaminathan *et al.*, 1997). The energy-filtered data were obtained using a serial electron energy-loss spectrometer and a scanning unit (Zuo *et al.*, 1993; Saunders *et al.*, 1995; Swaminathan *et al.*, 1997), an Ω filter (Deininger *et al.*, 1994; Cheng *et al.*, 1996) and a post-column filter (Saunders *et al.*, 1996). All these instruments are limited to detect diffraction intensities at small scattering angles. Thus, these cannot be applied to our method which uses the intensities of HOLZ reflections at high scattering angles. An energy filter with a high acceptance angle is needed for our method. The distortion of the CBED patterns due to aberrations of the lenses and the energy filter is appreciable for HOLZ reflections in the existing filters, though they are disregarded for zeroth-order Laue-zone (ZOLZ) reflections at small scattering angles. Small distortion is important for the accurate fitting of HOLZ reflection intensities. For these purposes, we have developed a new Ω-filter microscope, which can take CBED patterns up to a high angle with small distortion (Tsuno *et al.*, 1997; Tanaka *et al.*, 1998).

The use of two-dimensional CBED intensities provides much more information on structural parameters. It enables accurate fitting between experimental and theoretical intensities and thus improves the accuracy and reliability of the analysis. Saunders *et al.* (1995, 1996) first used zone-axis two-dimensional CBED patterns for the measurement of low-order structure factors. They reported that low-order structure factors of Si were determined from a [110] zone-axis energy-filtered CBED pattern with accuracy comparable to the X-ray *Pendellösung* method (Lu *et al.*, 1993). It should be noted that they did not carry out a distortion correction of the patterns because they used only ZOLZ reflections near the optical axis of the microscope. We again emphasize that distortion correction is unavoidable for two-dimensional intensity fitting of HOLZ reflections.

The purpose of this paper is to describe our new procedure to refine structural parameters using two-dimensional energy-filtered CBED patterns through the structure refinement of CdS as a test example.

2. Analysis procedure

2.1. *A new Ω-filter electron microscope*

Tsuda & Tanaka (1995) pointed out that the use of energy-filtered CBED patterns of HOLZ reflections is indispensable for structure refinement by the CBED method. The new Ω-filter transmission electron microscope JEM-2010FEF that we have developed (Tsuno *et al.*, 1997; Tanaka *et al.*, 1998) is equipped with a Schottky-type field-emission gun as the electron source and a newly designed Wollnik-type Ω filter. The microscope attains a 0.19 nm point-to-point resolution and a 0.5 nm probe on a specimen with the use of a pole piece of the objective lens with $C_s = 0.5$ mm. The Ω filter has energy dispersions of 2.1 and 1.1 μm eV^{-1} at accelerating voltages of 100 and 200 kV, respectively. The microscope can take CBED patterns up to an angle of 9° at 100 kV with an energy window of ±8 eV, the distortion of the pattern being less than 1%. It enables us to take energy-filtered CBED patterns including HOLZ reflections for the first time.

We use imaging plates (IP) of Fuji type FDL-UR-V to record CBED intensities. The IP has a dynamic range of five digits (10^{-18}–10^{-13} C m^{-2}) and a linear response with electron doses (Mori *et al.* 1988). The recorded intensities are read out by an He–Ne laser beam of an imaging-plate reader of Fuji type FDL-5000, and transferred to a Macintosh computer as a digitized pattern with 16 384 logarithmic signal levels and 3000 × 3760 pixels. The size of each pixel is 25 × 25 μm. The microscope uses a high-definition TV camera for real-time observation instead of human eye observation of images on a fluorescent screen and uses a multiscan charge-coupled-device (CCD) camera for detailed observation or precise focusing. The microscope is separated from its control console, and thus all apertures, the energy slit and the specimen stage being remote-controlled. The microscope is set on an air-spring mount with an active vibration cancel system.

2.2. *Pre-processing of experimental intensity data*

Two-dimensional intensity distributions of HOLZ reflection discs are taken out of the recorded patterns on the computer. Instead of one-dimensional line-profile data, two-dimensional data, or azimuthal intensity variation in reflection discs, provide a great increase of the number of data points, which enables us to conduct the accurate crystal structure refinement.

2.2.1. *Correction of distortion of CBED patterns*. To use two-dimensional HOLZ intensities, it is necessary to correct the distortion of a CBED pattern due to aberrations of the lenses and the Ω filter of the electron microscope. The distortion due to the lenses can be described by radial and spiral distortions (Tsuda & Tanaka, 1995). The displacements Δr of the radial distortion along the radial direction and Δs of the spiral

distortion along the azimuthal direction are expressed by $\Delta r = C_r r^3$ and $\Delta s = C_{sp} r^3$, where r is the distance from the optical axis, and C_r and C_{sp} are the coefficients of the radial and spiral distortions, respectively. The distortion due to the Ω filter are well approximated to be elliptical. That is, the displacements Δe_x and Δe_y of the elliptical distortion along the x and y axes are given by

$$\Delta e_x = C_{el}[r\cos(t+\theta)\cos\theta + r\sin(t+\theta)\sin\theta]$$

and

$$\Delta e_y = -C_{el}[-r\cos(t+\theta)\sin\theta + r\sin(t+\theta)\cos\theta] \times (C_{el}+1)^{-1},$$

where θ is the angle between the major axis of the ellipse of the distortion and the x axis, t is the angle from the major axis, r is the distance from the optical axis and C_{el} is the coefficient of the elliptical distortion.

We have corrected the distortion of a CBED pattern itself using the above equations with the distortion coefficients determined from the positions of reflection discs. The procedure is as follows:

(*a*) The central positions of all reflection discs on a recorded CBED pattern are determined from the perimeters of the discs.

(*b*) Distortion coefficients of the radial, spiral and elliptical distortions are determined from the central positions determined above by the nonlinear least-squares fitting.

(*c*) The distortions of the CBED pattern are corrected by the equations using the distortion coefficients determined above.

An example of the correction of the distortion is shown in Fig. 1. Figs. 1(*a*) and 1(*b*) are the same part of a CBED pattern of CdS including HOLZ reflection discs. The calculated positions of the HOLZ reflections are indicated by black circles. Figs. 1(*a*) and 1(*b*), respectively, show the positions without and with correction for distortion. It is seen that the positions of the circles agree much better with the perimeters of the HOLZ reflections in Fig. 1(*b*).

2.2.2. *Background subtraction due to phonon scattering*. Energy-filtered CBED patterns still contain weak diffuse background intensity and Kikuchi lines and bands, which are formed by phonon scattering. We assumed that background intensity distribution in each reflection disc changes linearly along the lines parallel to the Kikuchi line or band which crosses the reflection disc or is nearest to it. Background intensities in each reflection disc were subtracted by linear interpolation between the background intensities just outside the disc along the lines. In the present analysis, we omitted the parts of the reflection discs in which more than two Kikuchi lines or bands intersect.

2.2.3. *Evaluation of experimental error*. Experimental error σ_{exp} of an intensity in a reflection disc consists of the counting error σ_{IP} of the IP and the error σ_{bg} that arises when evaluating the background described above. The error σ_{IP} is well approximated to be $\sigma_{IP} = (I_{obs})^{1/2}$, where I_{obs} is a raw intensity in the disc. The error σ_{bg} is the standard deviation of the intensity just outside the reflection disc. The experimental error σ_{exp} for the background-subtracted intensity I_{exp} is given by $\sigma_{exp}^2 = \sigma_{IP}^2 + \sigma_{bg}^2$.

2.3. *Calculation*

Theoretical intensities of CBED patterns are obtained by many-beam dynamical calculations. The structural parameters are refined so as to minimize the residual sum of squares between the experimental CBED intensities and the theoretical ones. For such calculations, we have developed a C program (*MBFIT*: many-beam dynamical calculations and least-squares fitting). The features and functions of the program are described below.

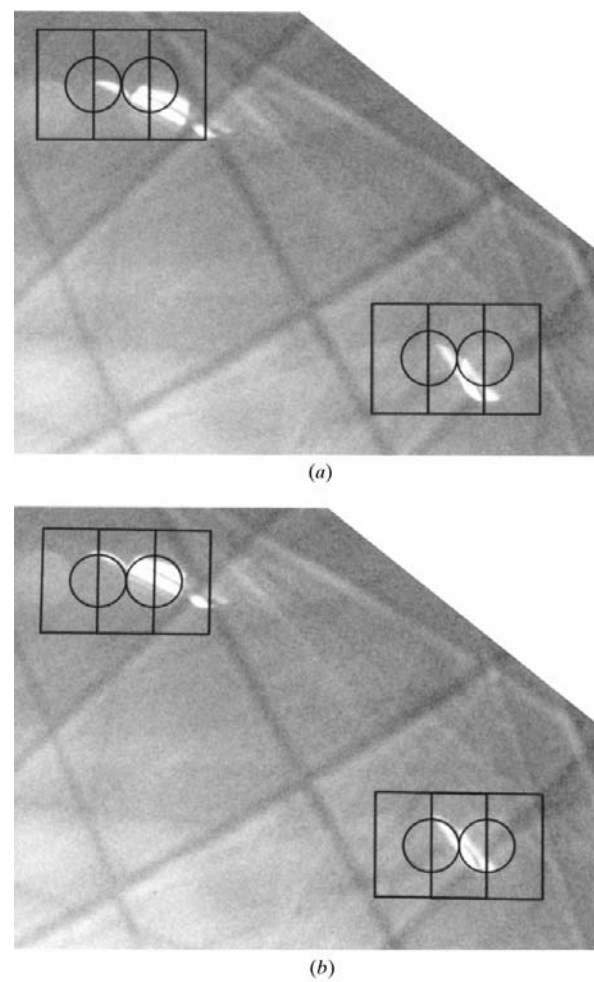

Fig. 1. Example of correction of distortion: a part of a CBED pattern of CdS including HOLZ reflection discs. The positions of the HOLZ reflections are indicated by black circles (*a*) without and (*b*) with correction of distortion.

2.3.1. *Dynamical calculation*. The intensity calculation is based on the Bloch-wave formulation of dynamical theory, namely matrix diagonalizations of many-beam equations (*e.g.* Bethe, 1928; Hirsch *et al.* 1977; Jones *et al.*, 1977; Spence & Zuo, 1992). Crystal potentials used for the many-beam equation are calculated using electron atomic scattering factors of Doyle & Turner (1968), atom positions, Debye–Waller factors and site occupancies. The electron atomic scattering factors are calculated not by a Gaussian parameterization as described in the paper of Doyle & Turner (1968) but by a quadratic interpolation (Bird & King, 1990) to obtain accurate values at scattering angles higher than $g/2 = 2.0$ Å^{-1}, where **g** is the scattering vector. Symmetrically equivalent atom positions are automatically generated using space-group symmetries. The program contains tables of electron atomic scattering factors and space-group symmetries.

Absorption due to inelastic scattering is taken into account using an absorption (imaginary) potential. The contribution of thermal diffuse scattering to the imaginary potential, which is the most significant, has been calculated using the Einstein model of lattice vibrations (Hall & Hirsch, 1965; Bird & King, 1990; Weickenmeier & Kohl, 1991; Allen & Rossouw, 1990; Peng *et al.*, 1996*a*,*b*). We have employed the imaginary potential given by the subroutine *ATOM* (Bird & King, 1990). To obtain accurate intensities of HOLZ reflections, the imaginary potential is treated not by perturbation but by exactly solving the matrix of the dynamical theory.

The reflections used in the scattering matrix are selected so that the values of their excitation errors s_g and reciprocal vectors **g** respectively satisfy $s_g < s_{\max}$ and $g < g_{\max}$. It is noted that magnitudes of their structure potentials U_g are not used for the selection criterion because even forbidden reflections with $U_g = 0$ are often important through dynamical interaction. When intensities are calculated with variation of the incident-beam direction to obtain a CBED pattern, the reflections used are selected differently for each incident direction because the excited reflections change with the incident directions.

The generalized-Bethe-potential (GBP) method (Ichikawa & Hayakawa, 1977) is adopted to reduce the dynamical calculation time, as already described in a paper of Tsuda & Tanaka (1995). In the GBP method, the effects of weakly excited beams are incorporated into the crystal-potential coefficients of strongly excited beams, thereby the order of the initial matrix to be diagonalized being reduced. The GBP method gives more accurate intensities than the original Bethe-potential method because the former includes all the higher-order Bethe-potential terms, which are neglected in the latter. The reflections with excitation errors $s_g \leq s_{s\max}$ are regarded as the strongly excited reflections and those with $s_{s\max} < s_g \leq s_{w\max}$ the weakly excited ones. That is, ZOLZ reflections appearing at the outer part of a CBED pattern are treated as the weakly excited ones.

2.3.2. *Nonlinear least-squares fitting*. The structural parameters are refined so as to minimize the residual sum of squares S between the experimental CBED intensities and the theoretical ones by a nonlinear least-squares fit. The quantity S is defined as

$$S = \sum_i w_i [I_i^{\exp} - s I_i^{\mathrm{cal}}(\mathbf{x})]^2, \qquad (1)$$

where $I_i^{\exp}$ is the ith experimental intensity, which is pre-processed as described in §2.2, I_i^{cal} is the calculated intensity corresponding to $I_i^{\exp}$ for all the structural parameters **x**, w_i is a weight factor and s is a scale factor common to all the calculated intensities.

We have set the weight factor $w_i = w_{\mathrm{LZ}}/(\sigma_i^{\exp})^2$, where $\sigma_i^{\exp}$ is the experimental error of $I_i^{\exp}$ and is evaluated as described in §2.2.3. w_{LZ} is an additional weight factor to decrease the weight of ZOLZ reflections in the residual sum of squares S: $w_{\mathrm{LZ}} = 1.0$ for HOLZ reflections and $w_{\mathrm{LZ}} \sim 0.001$ for ZOLZ reflections. Both the HOLZ reflections and ZOLZ reflections are necessary to determine the Debye–Waller factors because the scattering angles of the HOLZ reflections are almost the same and thus the scale factor and the Debye–Waller factors cannot be determined at the same time from only HOLZ reflections. Since intensities of ZOLZ reflections are more than 10^2 times those of HOLZ reflections and rather insensitive to positional parameters, the weights of ZOLZ reflections should be decreased using w_{LZ} for precise determination of the positional parameters. We have determined the values of w_{LZ} so that

$$\sum_{\mathrm{ZOLZ}} w_i (I_i^{\exp})^2 \Big/ \sum_{\mathrm{HOLZ}} w_i (I_i^{\exp})^2 = 0.1. \qquad (2)$$

Minimization of S is performed by the Levenberg–Marquardt method (*e.g.* Press *et al.*, 1989), which is known as a standard algorithm of the nonlinear least-squares fitting. The fitting starts from a set of initial values of the structural parameters and continues until S reaches a minimum. Structural parameters (atom positions, Debye–Waller factors and site occupancies), a scale factor common to all the calculated intensities, a specimen thickness, low-order structure factors and geometrical parameters are refined at the same time in the fitting. The geometrical parameters are introduced for correcting the small residual displacements of reflection discs, which exist even after the correction of the pattern distortion described in §2.2.1. The standard deviations of the refined parameters are evaluated according to the error propagation rule as already described in Tsuda & Tanaka (1995).

In order to incorporate the instrumental function or the effect of blurring due to the aberration of electron optical lenses, especially of the Ω filter and the detection

device of the IP, we have convoluted a Gaussian function $\exp(-a^2/x^2)$ into the calculated patterns.

The Levenberg–Marquardt method requires gradients of the theoretical intensities as a function of the fitting parameters, as the quasi-Newton method employed by Saunders *et al.* (1995) does. They developed analytical expressions of the gradients to reduce the calculation time. Unfortunately, their expressions cannot be used for the present analysis because those are restricted to two-dimensional Bloch-wave calculations, or not applicable to HOLZ reflections. We have applied a perturbation method proposed by Zuo (1991) to the evaluation of the gradients for cases including HOLZ reflections. That is, intensity changes caused by small changes of structural parameters are calculated by the perturbation method without a new diagonalization of the scattering matrix, where the gradients are calculated from the intensity changes under a finite difference approximation. This method allows a large increase of the number of structural parameters without a great increase of computing time.

Similar to conventional X-ray structure analysis, the reliability factor

$$R_w = \left[\sum_i w_i (I_i^{\exp} - s I_i^{\mathrm{cal}})^2 \Big/ \sum_i w_i (I_i^{\exp})^2 \right]^{1/2} \qquad (3)$$

and the goodness of fit (GOF)

$$\mathrm{GOF} = \left[\sum_i w_i (I_i^{\exp} - s I_i^{\mathrm{cal}})^2 \Big/ (N - M) \right]^{1/2} = R_w / R_e \qquad (4)$$

are calculated, where N is the number of data points and M is the number of parameters to be refined. The GOF is sometimes referred to as the χ factor. R_e is the expected value of R_w and is defined as

$$R_e = \left[(N - M) \Big/ \sum_i w_i (I_i^{\exp})^2 \right]^{1/2}.$$

A GOF value of 1 indicates that the fitting is perfect.

3. Performance test: CdS

3.1. *Structure of CdS*

We have selected cadmium sulfide (CdS) as a test material for developing the present analysis method. CdS is a semiconducting material with pyroelectricity and possesses the noncentrosymmetric hexagonal wurtzite structure belonging to space group $P6_3mc$. The atomic coordinates are expressed as Cd: $(1/3, 2/3, 0)$, $(2/3, 1/3, 1/2)$ and S: $(1/3, 2/3, u)$, $(2/3, 1/3, 1/2 + u)$, where u is the ratio of the distance between the adjacent Cd and S atoms along the c axis and the lattice parameter c (Fig. 2). The structural parameters to be refined in this analysis are u and isotropic Debye–Waller factors B(Cd) and B(S) as the first step. Anisotropic Debye–Waller factors B_{11} and B_{33} for both atoms are determined at the second stage. The lattice parameters used are $a = 4.136$ and $c = 6.713$ Å (National Bureau of Standards, 1955).

3.2. *Experimental*

Thin foil specimens for transmission electron microscopy were prepared by chemical polishing using hot phosphoric acid. CBED experiments were conducted using a JEM-2010FEF as already described. The accelerating voltage of the electron microscope was determined to be 100.7 kV using a HOLZ line pattern of silicon, the method being described in a paper by Tsuda & Tanaka (1995).

CBED patterns taken at incidences $[UV0]$ (U, V integers) are sensitive to parameter u of S atoms because parameter u is parallel to the c axis. The HOLZ reflection intensities of the patterns taken at incidences of [100] (equivalent to [010] and [110]) and [210] (equivalent to [120] and [110]) are too weak to analyze. Those at incidences [310] and [410] are relatively strong, but less HOLZ reflections are excited at incidence [410]. For these reasons, we used [310] CBED patterns for the determination of the structural parameters.

3.3. *Bloch states of CdS*

Prior to the fitting between experimental and theoretical data, we interpret intensity distributions of HOLZ reflections in terms of Bloch waves (Kambe *et al.* 1974; Buxton, 1976; Jones *et al.*, 1977; Buxton *et al.*, 1978; Tsuda & Tanaka (1995).

Fig. 3(*a*) shows a section of the *dispersion surface* around the [310] incidence along the c^* axis. The line profile of the 0,1,15 reflection is shown in Fig. 3(*b*). For simplicity, the dispersion surface was calculated using only one HOLZ reflection 0,1,15 and 101 ZOLZ reflections for an accelerating voltage of 100 kV. The

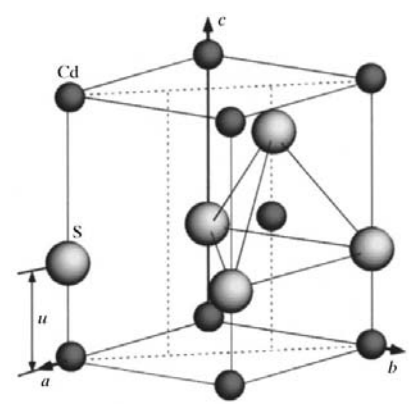

Fig. 2. Crystal structure of CdS. The coordinates of the atoms shown here are displaced from those described in the text by $(-1/3, 1/3, 0)$ to clarify the arrangement of the atoms.

branch of the dispersion surface originating from the HOLZ reflection is clearly distinguished from those of ZOLZ reflections because the HOLZ branch makes a large angle with the ZOLZ branches, which lie almost perpendicular to the [310] direction. Intensity peaks of the HOLZ reflection appear at the intersections between HOLZ and ZOLZ branches. It should be noted that only well excited ZOLZ branches with large excitation amplitudes $\varepsilon^{(j)}$ cause intensity peaks in the HOLZ reflection. In the present case, the three peaks of the line profile seen in Fig. 3(*b*) are assigned to the intersection between the HOLZ branch and the ZOLZ branches 1, 4 and 5. The other small peaks can be regarded as subsidiary peaks of the three principal peaks.

Figs. 4(*a*) and 4(*b*) show the projected structure and projected potential of CdS along the [310] direction, respectively. It is seen that the projected structure consists of rows of Cd atoms and rows of S atoms. Figs. 4(*c*)–4(*e*) show electron-density distributions of the Bloch waves corresponding to branches 1, 4 and 5, respectively, which were calculated using 101 ZOLZ reflections at [310] incidence for an accelerating voltage of 100 kV. The electron density of branch 1 is concentrated on the rows of Cd atoms (Fig. 4*c*), that of branch 4 mainly on the rows of S atoms and weakly on those of Cd atoms (Fig. 4*d*) and the electron density of branch 5 is between the rows of Cd and S atoms (Fig. 4*e*). The branch that has electron density maxima on rows of both Cd and S atoms should be sensitive to the relative distance u between Cd and S atoms. That is, the intensity peak of the HOLZ reflection due to branch 4 is most sensitive to parameter u.

Fig. 5 shows the squares of the excitation amplitudes of the branches around the [310] incidence as a function of $\mathbf{k}_{xy}$, where $\mathbf{k}_{xy}$ is the component of the incident wavevector along the c^* axis. It is seen that the excitation of branch 4 has maxima around $\mathbf{k}_{xy} = \pm 3\mathbf{g}_{002}/4$, where reflections 003 and $00\bar{3}$ are respectively in Bragg condition. Therefore, CBED patterns taken at the incidences to excite these reflections are expected to show strong intensity peaks due to branch 4 and thereby a high sensitivity to parameter u.

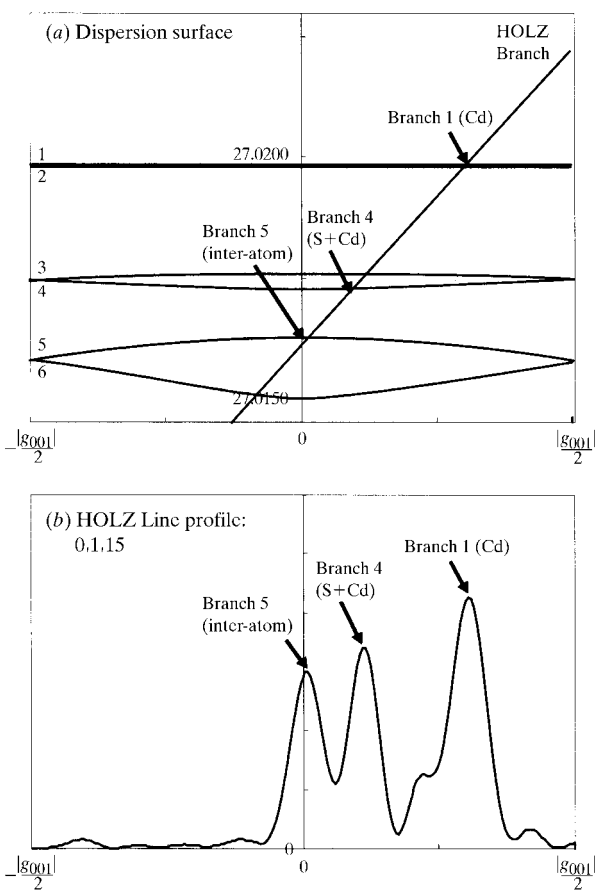

Fig. 3. (*a*) Branches of dispersion surfaces of CdS around the [310] incidence. (*b*) The corresponding line profile of the 0,1,15 HOLZ reflection. Peaks of the line profile appear at the intersections of the HOLZ branch and the ZOLZ branches of 1, 4 and 5.

3.4. *Fitting*

Considering the features described in the previous subsection, we took CBED patterns with the incidences slightly tilted from the [310] zone axis so that the 002 and $00\bar{2}$ reflections satisfied their Bragg conditions. Fig. 6 shows a CBED pattern of CdS taken with the 002 Bragg condition at room temperature. The pattern was taken from about a 1 nm-diameter area with an acceptance energy of 0 ± 8 eV, where the acceptance angle of the pattern was about 8°. ZOLZ reflections are seen at the center of the pattern and HOLZ reflections as a ring in the outer part. The remaining background intensities outside the reflection discs were approximately 2% of the intensity maxima inside them for the ZOLZ reflections and approximately 10% for the first-order Laue-zone (FOLZ) reflections.

After such distortion correction and background subtraction as described in §2, two-dimensional intensities of four ZOLZ reflections and twenty FOLZ reflections were taken out of the CBED pattern. The specimen thickness was determined to be 930 Å by comparing the experimental ZOLZ CBED patterns with calculated ones, where parameter u of 0.375 and Debye–Waller factors B(Cd) and B(S) of 1.0 Å^2 were assumed. This value of the specimen thickness was used as a starting value to refine all parameters. The number of total data points in the present pattern was 36 252, which is much greater than those for line profiles. The weight factor w_{LZ} for ZOLZ reflection intensities was set to be 0.0015 according to the ratio of $\sum w_i I^2$. From the results of the convergence tests of intensities with the number of reflections, 279 reflections were taken for the dynamical calculations according to the procedure

described in §2.3.1 with the parameters of $g_{max} = 4.0$, $s_{s\,max} = 0.015$ and $s_{w\,max} = 0.03$ Å^{-1}. 119 weak reflections among the 279 reflections were treated by the GBP method.

The parameters to be refined in the fitting are structural parameters u, B(Cd) and B(S), scale factor s, specimen thickness t and 28 geometrical parameters to adjust the positions of the reflection discs. The nonlinear least-squares fitting was converged in three iterations. The fitting took about 15 h on a DEC Alpha workstation. Fig. 7 shows the final result of the fitting between experimental and calculated reflection patterns. The patterns in the left, center and right columns, respectively, show experimental, calculated and difference patterns. Calculated patterns are seen to agree very well with experimental ones. It should be noted that large intensity variations along the azimuthal directions as seen in reflections $2,\bar{5},\bar{12}$, $2,\bar{5},14$ and $1,\bar{2},16$ were well reproduced in the calculated patterns. If such reflections are used for line-profile fitting, the intensity distribution of the line profile is very sensitive to the azimuthal position. The intensity fitting for such line profiles is not reliable. Thus, two-dimensional fitting is required for accurate refinement. The refined values of the structural parameters were $u = 0.37775\,(2)$, $B(\mathrm{Cd}) = 1.492\,(1)$ and $B(\mathrm{S}) = 1.079\,(2)$ Å^2 with thickness $t = 915.0\,(3)$ Å and reliability factors $R = 0.081$, $R_w = 0.227$ and GOF = 1.61. This value of GOF implies that the fitting is very good.

Subsequently, we refined the parameters using anisotropic Debye–Waller factors $B(\mathrm{Cd})_{11}$, $B(\mathrm{Cd})_{33}$, $B(\mathrm{S})_{11}$ and $B(\mathrm{S})_{33}$ instead of the isotropic ones, though R_w obtained above may not be small enough for considering the anisotropic effect. The values of the parameters obtained above were used as the starting values in this fitting. The refined values were $u = 0.37797\,(2)$, $B(\mathrm{Cd})_{11} = 1.437\,(2)$, $B(\mathrm{Cd})_{33} = 1.517\,(2)$, $B(\mathrm{S})_{11} = 0.965\,(4)$ and $B(\mathrm{S})_{33} = 1.264\,(3)$ Å^2 with thickness $t = 913.3\,(3)$ Å and reliability factors $R = 0.083$, $R_w = 0.220$ and GOF = 1.56. A small improve-

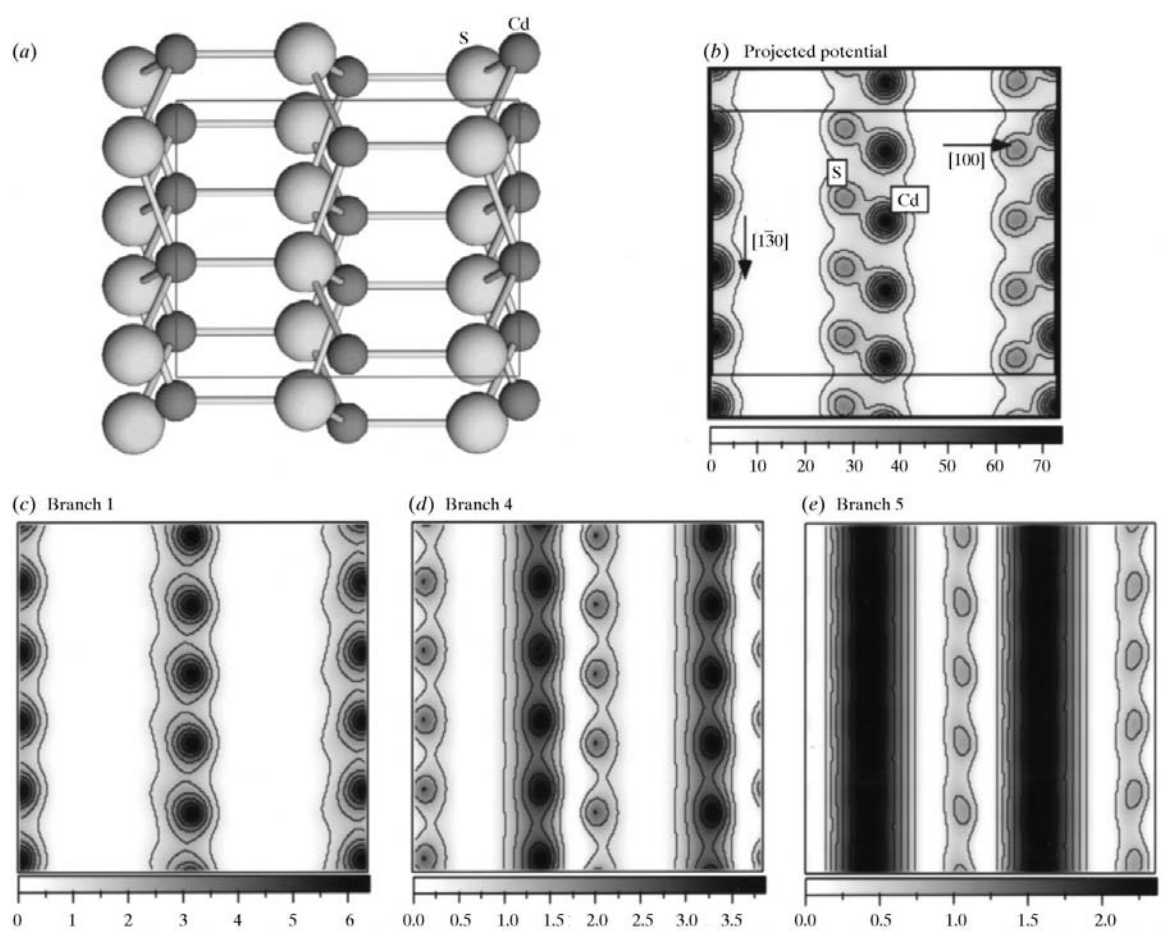

Fig. 4. (*a*) Projected structure of CdS along the [310] zone axis, (*b*) projected potential distribution, (*c*)–(*e*) electron-density distributions of the Bloch waves of branches 1, 4 and 5, respectively. It should be noted that the electron-density maxima are located on rows of both Cd and S atoms.

ment of R_w and GOF is seen with a small change of parameter u.

Fig. 8 shows another CBED pattern of CdS taken with the $00\bar{2}$ Bragg position at room temperature using the JEM-2010FEF. The pattern was taken from about 1 nm-diameter area with an acceptance energy of 0 ± 8 eV, similar to Fig. 6. In a similar manner as described above, the structural parameters were refined using this pattern independently from Fig. 6. The final result of the fitting is shown in Fig. 9 with the use of the isotropic Debye–Waller factors. The number of total data points in the present pattern was 32 099. The refined values were $u = 0.37707\,(2)$, $B(\mathrm{Cd}) = 1.430\,(1)$ and $B(\mathrm{S}) = 1.119\,(2)$ Å^2 with thickness $t = 935.0\,(3)$ Å and reliability factors $R = 0.172$, $R_w = 0.208$ and GOF $= 1.836$. For the anisotropic Debye–Waller factors, they were $u = 0.37751\,(2)$, $B(\mathrm{Cd})_{11} = 1.371\,(2)$, $B(\mathrm{Cd})_{33} = 1.486\,(2)$, $B(\mathrm{S})_{11} = 1.135\,(5)$ and $B(\mathrm{S})_{33} = 1.155\,(4)$ Å^2 with thickness $t = 935.7\,(3)$ Å and reliability factors $R = 0.168$, $R_w = 0.208$ and GOF $= 1.765$.

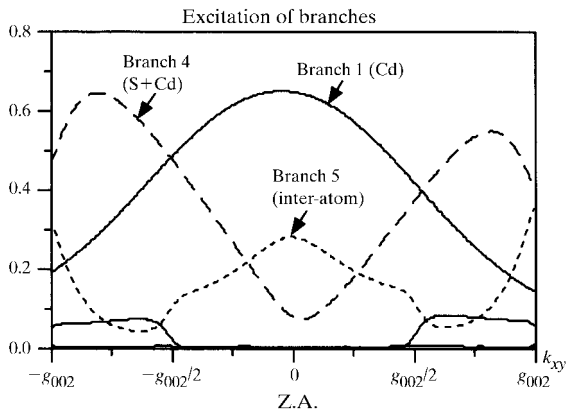

Fig. 5. Excitation amplitudes of Bloch states as a function of $\mathbf{k}_{xy}$.

Table 1 shows the avaraged values of the structural parameters of the two results described above. The present results agree with the results of a single-crystal X-ray diffraction experiment, $u = 0.37715\,(8)$, $B_{\mathrm{equiv}}(\mathrm{Cd}) = 1.394\,(4)$ and $B_{\mathrm{equiv}}(\mathrm{S}) = 1.133\,(12)$, $B(\mathrm{Cd})_{11} = 1.376\,(3)$, $B(\mathrm{Cd})_{33} = 1.430\,(5)$, $B(\mathrm{S})_{11} = 1.136\,(7)$ and $B(\mathrm{S})_{33} = 1.126\,(20)$ Å^2 (Stevenson *et al.*, 1984), except for small discrepancies of anisotropic B factors.

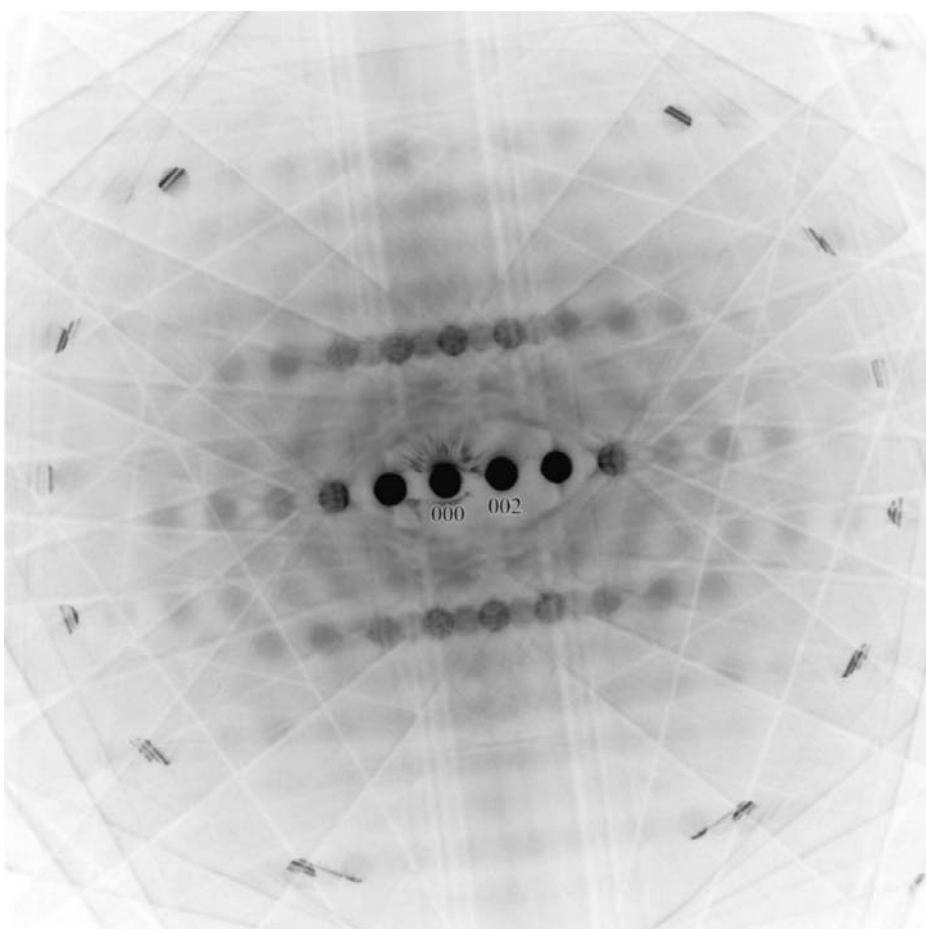

Fig. 6. CBED pattern of CdS taken with the 002 Bragg position slightly tilted from the [310] zone axis at room temperature.

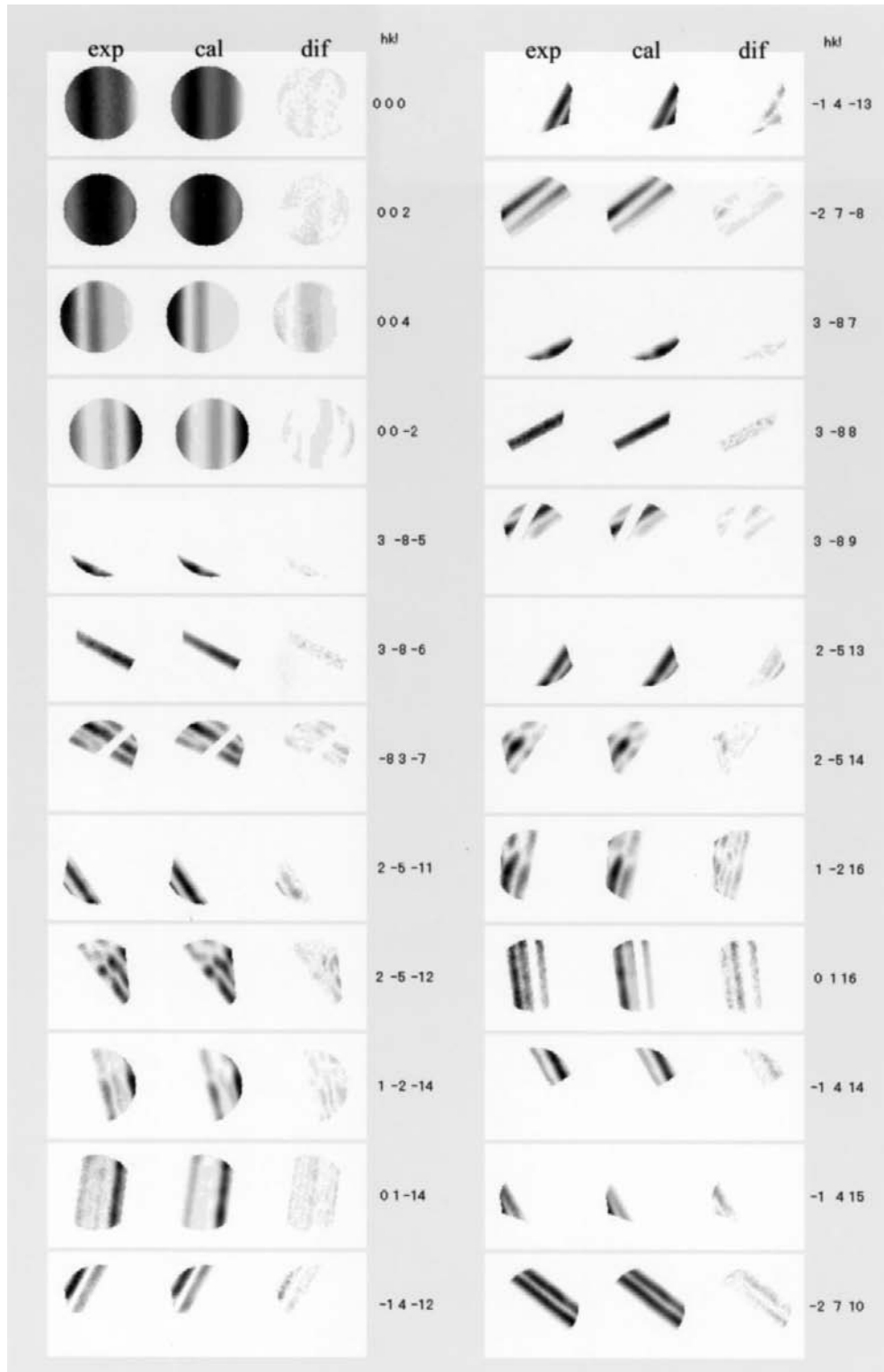

Fig. 7. Final result of the fitting using the data of Fig. 6 taken with the 002 Bragg position. The patterns in the left, center and right columns respectively show experimental, calculated and difference patterns.

Table 1. *The averaged values of the structural parameters obtained from the two data sets taken for the 002 and 00$\bar{2}$ Bragg positions (Figs. 6 and 8)*

Parameter	Present result	X-ray results (Stevenson *et al.*, 1984)
u	0.3774 (3)	0.37715 (8)
B(Cd) (Å^2)	1.46 (3)	1.394 (4)
B(S) (Å^2)	1.10 (2)	1.13 (1)
B_{11}(Cd) (Å^2)	1.40 (3)	1.376 (3)
B_{33}(Cd) (Å^2)	1.50 (2)	1.430 (3)
B_{11}(S) (Å^2)	1.05 (8)	1.136 (7)
B_{33}(S) (Å^2)	1.21 (6)	1.126 (20)

In addition, we took CBED patterns at 90 K with the 002 Bragg condition using a liquid-nitrogen specimen-cooling holder. Second-order Laue-zone (SOLZ) reflections as well as first-order Laue-zone (FOLZ) reflections appeared in the pattern because thermal vibrations of the atoms were suppressed. In a similar manner, the structural parameters were refined using this pattern. The total number of data points in the present pattern was 61 401. The lattice parameters used for the low-temperature analysis are $a = 4.131$ and $c = 6.708$ Å, which were evaluated using the thermal expansion coefficients at room temperature. The lattice parameters at the low temperature are smaller than those at room temperature by about 0.1%. The refined values were $u = 0.377605\,(7)$, $B(\mathrm{Cd}) = 0.5261\,(2)$ and $B(\mathrm{S}) = 0.2854\,(3)$ Å^2 with thickness $t = 496.34\,(5)$ Å and reliability factors $R = 0.217$, $R_w = 0.228$ and GOF $= 3.92$ with the use of isotropic Debye–Waller factors, and $u = 0.377\,757\,(7)$, $B(\mathrm{Cd})_{11} = 0.4551\,(3)$, $B(\mathrm{Cd})_{33} = 0.5839\,(4)$, $B(\mathrm{S})_{11} = 0.3412\,(7)$ and $B(\mathrm{S})_{33} = 0.2615(5)$ Å^2 with thickness $t = 496.65\,(5)$ Å and reliability factors $R = 0.214$, $R_w = 0.222$ and GOF $= 3.80$ with the use of anisotropic Debye–Waller factors. It is noted that parameter u is almost the same as that at room temperature. The Debye–Waller factors at 90 K are nearly one third of those at room temperature, which are reasonable from the temperature ratio. The value of GOF is greater than those at room temperature although the values of R_w are comparable. This is mainly due to the relatively higher signal-to-noise ratio of the data at 90 K, or a lower value of R_e (§2.3.2).

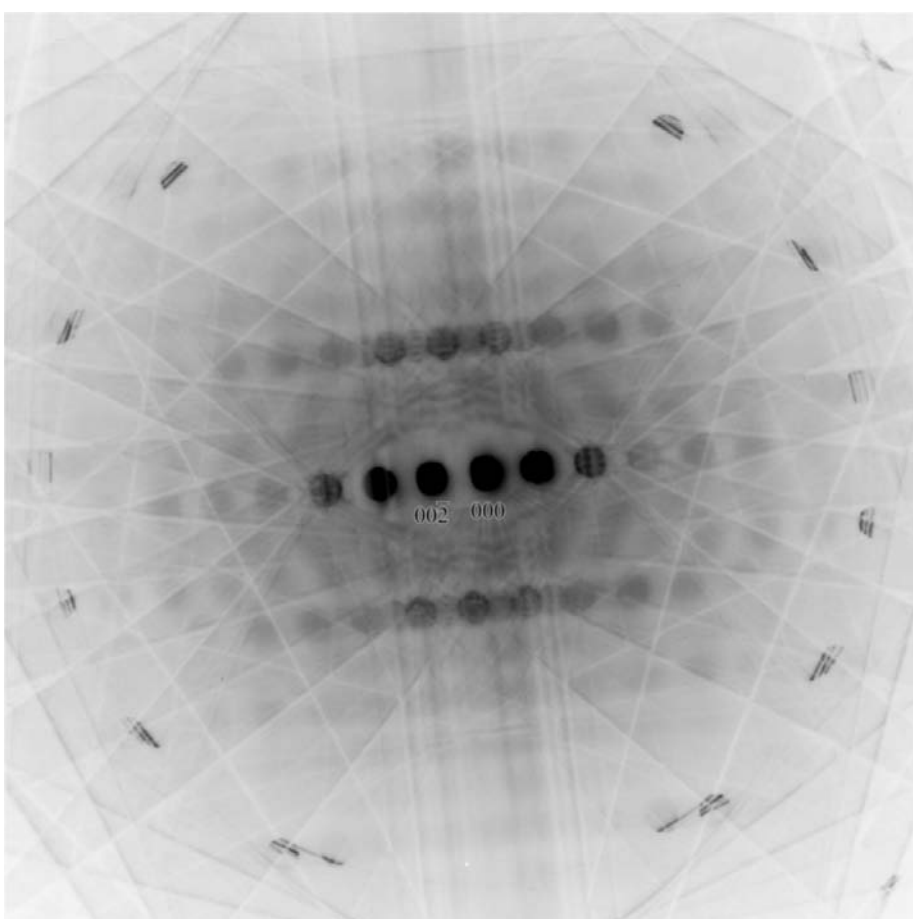

Fig. 8. CBED pattern of CdS taken with the 00$\bar{2}$ Bragg position slightly tilted from the [310] zone axis at room temperature.

4. Discussion

4.1. *Plots of R_w as a function of parameter u*

To check the existence of local minima in the fitting, we plotted the values of R_w against parameter u. Fig. 10 shows the plots of R_w, R_w^{ZOLZ} and R_w^{HOLZ} for the data of Fig. 6, which were taken under the 002 Bragg condition at room temperature, where R_w^{ZOLZ} and R_w^{HOLZ} were calculated from the data of ZOLZ reflections and HOLZ reflections, respectively. Since all R_w's show no local minima, the values of the parameters obtained are the unique solution corresponding to the global

Fig. 9. Final result of the fitting using the data of Fig. 8 taken with the 00$\bar{2}$ Bragg position.

minimum. It should be noted that the R_w^{HOLZ} curve shows a deep minimum, but the R_w^{ZOLZ} curve shows a shallow minimum at a u value that is little different from that of R_w^{HOLZ}. This shows that the HOLZ reflections are more sensitive to parameter u than the ZOLZ reflections. Thus, the use of HOLZ reflections is indispensable for determination of structural parameters.

The curves of R_w and R_w^{HOLZ} are very close and have the minima at the same position, because the weight factor w_{LZ} was set to a small value. With the increase of w_{LZ} for ZOLZ reflections, the curve R_w approaches that of R_w^{ZOLZ}, which makes difficult the accurate determination of positional parameters. On the other hand, when w_{LZ} is decreased to a very small value, the correlation between scale factor s and Debye–Waller factors B increases and thus unique determination of the parameters becomes unfeasible. The value ~ 0.001 of the weight factor w_{LZ} determined by equation (2) was obtained by a compromise of the two requirements.

4.2. *Instrumental function*

The aberration of the electron optical components, especially of the Ω filter, and the cross talk in the detection device IP can cause the blurring of CBED patterns. This blurring is treated as an instrumental function of the electron microscope. As described in §2.3.2, we have assumed a Gaussian function as the instrumental function, and have convoluted the Gaussian function into the calculated intensities. Table 2 shows the values of R factors and refined structural parameters without and with the use of the function. Considerable improvements of the R_w and GOF are seen when the function is used. The values of R_w were improved from about 0.3 to 0.2. The value of positional parameter u hardly changed but those of Debye–Waller factors came slightly closer to the values of an X-ray analysis (Stevenson *et al.*, 1984). Figs. 11(*a*) and 11(*b*) show the experimental (exp), calculated (cal) and difference (dif) line profiles of the $7\bar{2}\bar{8}$ HOLZ reflection (*a*) without and (*b*) with convolution. The convolution reduced the peak heights and valley depths of the calculated intensity profile, resulting in a better agreement with the experimental one.

It should be noted that the value of R_w^{ZOLZ} is also improved by the use of the function, although the

Table 2. *The values of R factors and refined structure parameters without and with the use of the instrumental function*

The upper and lower rows of R_w's and GOF indicate the values for the data taken at the 002 and $00\bar{2}$ Bragg positions, respectively.

Parameter	Without convolution	With convolution
R_w	0.318	0.227
	0.308	0.208
R_w^{ZOLZ}	0.182	0.135
	0.265	0.194
R_w^{HOLZ}	0.329	0.234
	0.312	0.209
GOF	2.26	1.61
	2.71	1.84
u	0.3773 (4)	0.3774 (3)
B(Cd) (Å^2)	1.50 (4)	1.46 (3)
B(S) (Å^2)	1.18 (3)	1.10 (2)

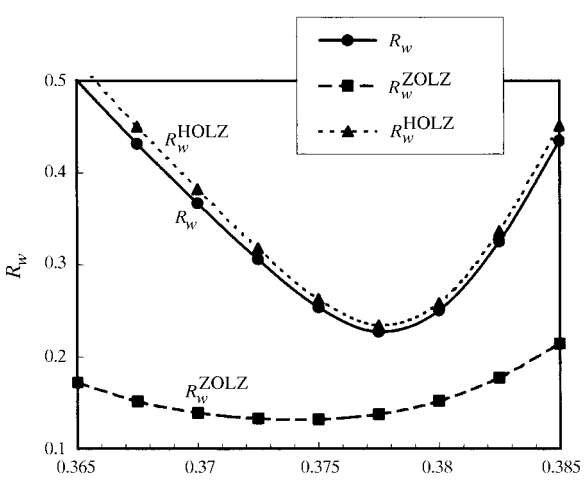

Fig. 10. Plots of R_w as a function of parameter u. Plots of R_w, R_w^{ZOLZ} and R_w^{HOLZ} for the data of Fig. 6 taken under the 002 Bragg condition at room temperature.

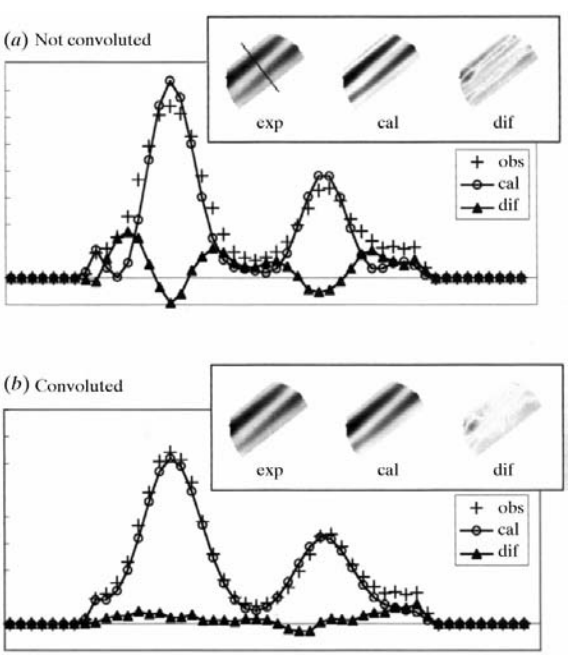

Fig. 11. Experimental (exp), calculated (cal) and difference (dif) line profiles of the $7\bar{2}\bar{8}$ HOLZ reflection (*a*) without and (*b*) with the convolution. The calculated line profile with the convolution clearly shows better agreement with the experimental one.

improvement of R_w^{ZOLZ} is smaller than that of R_w^{HOLZ} because the patterns of ZOLZ reflections are much broader than those of HOLZ reflections. This implies that the instrumental function should be taken into account even in measurements of the low-order structure factors using ZOLZ CBED patterns, although the effect of blurring due to the instrumental function has not been considered so far (Zuo *et al.*, 1989, 1993; Deininger *et al.*, 1994; Saunders *et al.*, 1995, 1996; Cheng *et al.*, 1996; Swaminathan *et al.*, 1997).

We emphasize that the instrumental function is necessary for quantitative fitting of CBED patterns, which is very important in the Rietveld method of X-ray and neutron diffraction techniques.

4.3. *Excitation of appropriate Bloch states*

We took CBED patterns with the incidences slightly tilted from the [310] zone axis instead of the zone axis incidence so that the 002 and $00\bar{2}$ reflections satisfied their Bragg conditions because the branch (Bloch state) that has electron-density maxima on rows of both the Cd and S atoms was strongly excited at these conditions. As a result, intensity peaks in HOLZ reflections attributed to the branch were increased and the sensitivity of the reflections to parameter u was increased. It should be noted that Fig. 5, where the squares of the excitation amplitudes of branches around the [310] incidence, shows that the branches 1, 4 and 5 are succesively excited with increasing the tilt of the incident beam from the zone axis. Thus, an appropriate tilt of the incident beam at which the sensitivity is high to specific positional parameters should be investigated by calculating the excitations of Bloch states as a function of tilt in advance of CBED experiments.

4.4. *Structural information contained in two-dimensional data*

Prior to the present fitting, we attempted refinements of the structural parameters using integrated intensity data (zero dimension) and intensity line-profile data (one dimension). In the former case, the parameters could not be determined at all because the fitting did not converge. In the latter case, the refined values of the parameters were different from those of an X-ray analysis (Stevenson *et al.*, 1984) when a set of the line profiles from one CBED pattern was used. When we used two data sets of the line profiles extracted from two CBED patterns taken with the incidences slightly tilted from the zone axis, we obtained the values of the parameters which agree well with the X-ray values. In addition to this, more than ten iterations were needed for the convergence in the nonlinear least-squares fitting. On the other hand, in the case of two-dimensional CBED pattern fitting, which has been made for the first time in the present study, a good fit was obtained between the two-dimensional intensities taken at the 002 excitation and theoretical calculations. The fitting provided the values of the parameters which are very close to those of the X-ray analysis. Furthermore, the convergence of the fitting was achieved by only three iterations. These facts clearly show that the two-dimensional data have much more structural information than zero- and one-dimensional data.

4.5. *Effective data points and standard deviations*

To obtain accurate intensity distribution of the CBED pattern and to refine the geometrical parameters, all the data points determined by the pixel number of an IP were used. In the present analysis, all the data points were also used for the refinement of the structural parameters. The standard deviations of the parameters obtained are appreciably underestimated because of the use of all the data points. Since the CBED pattern itself is formed by dynamical diffraction of a certain number of reflections, the number of independent data points for the determination of the structural parameters is considered to be, at the most, the number of reflections. We separately confirmed that we obtain larger standard deviation values with preservation of almost the same structural parameter values using the data points equal to the number of reflections.

4.6. *Subtraction of background intensities*

In the present energy-filtered data, the ratios of remaining background intensities outside the reflection discs to the intensity maxima in the discs were approximately 2% for the ZOLZ reflections and 10% for the FOLZ reflections. The present procedure of the background subtraction described in §2.2.2 works well for the areas with the monotonic background. Since the procedure does not work at the angular areas in a reflection disc where more than two Kikuchi lines or bands intersect, we did not use such areas for the fitting. Thus, the accuracy of the background subtraction is not a major contribution to the reliability factor or a value of $R_w \simeq 20\%$.

Theoretical calculation of the inelastic background pattern due to phonon scattering seems to be helpful but may not be accurate enough when the Einstein model is applied. It is in the course of examination whether the subtraction of calculated background is useful. The quantitative study of inelastic scattering is an important future problem.

4.7. *Convergence of many-beam calculations*

As described in §2.3.1, the reflections used in the scattering matrix are selected using the parameters $g_{\max}$, $s_{s\max}$ and $s_{w\max}$. The values of these parameters were determined as follows: Firstly, $g_{\max}$ was determined to be 4.0 $\mathrm{\AA}^{-1}$ so that the reflections up to the second-order Laue zone (SOLZ) were taken in. Secondly, from

preliminary test simulations without the use of the GBP method, $s_{w\max}$, which selects the set of total reflections, was set to be 0.03 Å^{-1}. Finally, the value of $s_{s\max}$ was set to be 0.015 Å^{-1} from test simulations so as to treat weak reflections using the GBP method. 279 reflections were selected as the total number under the values of parameters $g_{\max}$ and $s_{w\max}$, and 119 weak reflections among them were treated by the GBP method. In order to examine the convergence of calculations with these reflections, the calculated intensities were compared with the reference intensities calculated with 444 reflections. The 444 reflections were selected using the parameters of $g_{\max} = 4.0$, $s_{s\max} = 0.015$ and $s_{w\max} = 0.05$ Å^{-1}. In the reference calculation, 284 reflections of the reflections were treated by the GBP method. Like the case of Zuo & Weickenmeier (1995), the discrepancy between these two calculations was evaluated by χ^2 defined as

$$\sum_i \{(I_i^{\rm ref} - I_i^{\rm cal})^2 / I_i^{\rm ref}\}/(n-1),$$

where superscripts cal and ref represent, respectively, the intensities calculated with 279 and 444 reflections and n is the number of data points. The value of χ^2 was 0.20, which indicates that the discrepancy between the two calculations is sufficiently small. Furthermore, the structural parameters refined for the data of Fig. 6 using the 444 reflections were $u = 0.37743$, $B(\mathrm{Cd}) = 1.527$, and $B(\mathrm{S}) = 1.093$ Å^2. The differences between these values and those refined with 279 reflections shown in §3.4 are quite small. Therefore, the convergence of the calculation with 279 beams is sufficient for the structure refinement.

Let us consider two criteria $s_g\xi_g$ and s_g for selection of reflections. If the dimensionless excitation error $s_g\xi_g$ (ξ_g extinction distance) is used instead of s_g as a criterion, HOLZ reflections of large U_g with large s_g are selected, which locate on the 1st and −1st Laue zones near the zone axis. It was confirmed that the calculations with and without such HOLZ reflections agree well if such HOLZ reflections in both the Laue zones are selected symmetrically with respect to the zeroth Laue zone. This indicates that such HOLZ reflections make little contribution to the dynamical calculation because of their large s_g values. However, it was found that these two calculations do not agree if such reflections on either the 1st or the −1st Laue zone are selected. The two contributions from the 1st and −1st Laue zone reflections are canceled out in many-beam calculations. Thus, it is better to use criterion s_g, which selects no such HOLZ reflections. Furthermore, the criterion $s_g\xi_g$ cannot take forbidden reflections of $U_g = 0$ with small s_g because $s_g\xi_g = \infty$ for such reflections, such forbidden reflections often being important through dynamical interaction. As a conclusion, criterion s_g is appropriate for selection of reflections.

4.8. *Low-order structure factors*

The values of the low-order structure factors were fixed to those calculated from the atomic scattering factors for neutral atoms in the present analysis. The effect of the change of the low-order structure factors on the HOLZ reflection intensities was found to be negligible in the present case because there were few reciprocal vectors of the low-order reflections which connect the HOLZ reflections satisfying their Bragg conditions. If there are many HOLZ reflections which satisfy the above condition, accurate low-order structure factors have to be used or the low-order structure factors should be treated as fitting parameters.

4.9. *Thickness variation in the illuminated area*

If the convergent electron probe is exactly focused on the specimen, then experimental intensities are considered to be the intensities averaged over an illuminated area with thickness variation. However, we did not take into account the thickness variation. Thickness variation of the illuminated areas in the present experiments may be less than a few nm because the electron probe size used was approximately 1 nm in full width at half-maximum. Figs. 12(*a*)–12(*d*) show simulated line profiles of ZOLZ reflections 004, 002, 000 and 00$\bar{2}$ along the c^* direction with specimen thicknesses 88, 89, 90, 91 and 92 nm. It is seen that the line profile averaged over these five thicknesses with the same weight for each thickness is almost the same as the line profile of a thickness of 90 nm. Furthermore, HOLZ reflections which play an important role for the determination of parameter u

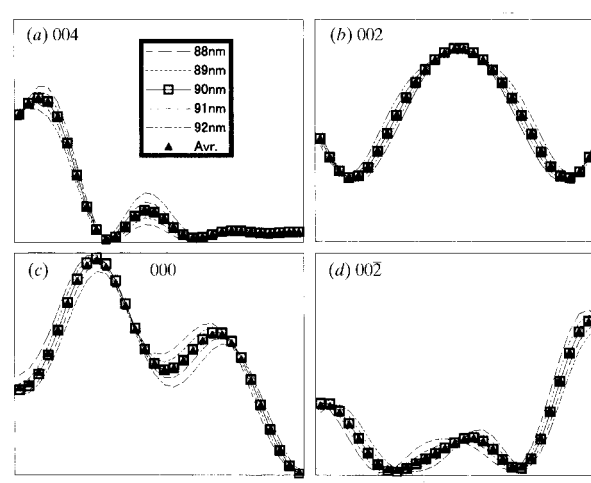

Fig. 12. Simulated line profiles of ZOLZ reflections 004, 002, 000, 00$\bar{2}$ and 00$\bar{4}$ along the c^* direction with specimen thicknesses 88, 89, 90, 91 and 92 nm. It is seen that the line profile averaged over these five thicknesses with the same weight for each thickness (filled triangles) is almost the same as the line profile of a thickness of 90 nm (squares).

are much more insensitive to thickness change than ZOLZ reflections because of their large extinction distances. For these reasons, a small thickness variation in the illuminated area does not affect the fitting result. Therefore, we can use the mean value of the thicknesses.

5. Concluding remarks

We have proposed a new procedure to refine structural parameters using two-dimensional Ω-filtered CBED patterns including HOLZ reflections. For this purpose, we have developed a new Ω-filter electron microscope JEM-2010FEF which can take energy-filtered CBED patterns up to a high angle with a small distortion, and a new analysis program *MBFIT* to refine structural parameters on the bases of many-beam dynamical calculations and nonlinear least-squares fitting. We have established a structure refinement procedure using CdS as a test example. We have pointed out that the selection of the incident-beam orientation to excite appropriate Bloch states is important and effective for increasing the sensitivity to certain positional parameters.

We are intending to apply this method to advanced materials, especially to perovskite-type transition-metal oxides, which show various structural transformations closely connected with their remarkable properties such as ferroelectricity, superconductivity and colossal magnetoresistance. These materials are frequently composed of minute twin domains in their low-temperature phases. The X-ray and neutron diffraction techniques are often difficult to obtain diffraction intensity data from a single domain but the CBED technique is easy. Thus, the present method can provide more reliable structural parameters for such materials with the help of correct space-group determination. The present method is also applicable to reveal the local structures around defects.

The authors are grateful to Ms N. Kanda and Mr K. Omoto for their considerable contributions in processing numerous CBED data, Dr K. Saitoh and Mr J. Shiono for their assistance in developing the analysis software *MBFIT*, and Mr F. Sato for his careful maintenance of the JEM-2010FEF. The present study was supported by a Grant-in-Aid for Specially Promoted Research of Ministry of Education, Science, Sports and Culture of Japan.

References

Allen, L. J. & Rossouw, C. J. (1990). *Phys. Rev. B*, **42**, 11644–11654.

Bethe, H. A. (1928). *Ann. Phys. (Leipzig)*, **87**, 55–129.

Bird, D. M. & King, Q. A. (1990). *Acta Cryst.* A**46**, 202–208.

Buxton, B. F. (1976). *Proc. R. Soc. London Ser. A*, **350**, 335–361.

Buxton, B. F., Loveluck, J. E. & Steeds, J. W. (1978). *Philos. Mag.* A**38**, 259–278.

Cheng, Y. F., Nüchter, W., Mayer, J., Weickenmeier, A. & Gjønnes, J. (1996). *Acta Cryst.* A**52**, 923–936.

Deininger, C., Necker, G. & Mayer, J. (1994). *Ultramicroscopy*, **54**, 15–30.

Doyle, P. A. & Turner, P. S. (1968). *Acta Cryst.* A**24**, 390–397.

Hall, C. R. & Hirsch, P. B. (1965). *Proc. R. Soc. London Ser. A*, **286**, 158–177.

Hirsch, P. B., Howie, A., Nicholson, R. B., Pashley, D. W. & Whelan, M. J. (1977). *Electron Microscopy of Thin Crystals*, 2nd ed., pp. 208–210. Florida: Krieger; London: Butterworth.

Ichikawa, M. & Hayakawa, K. (1977). *J. Phys. Soc. Jpn*, **42**, 1957–1964.

Jansen, J., Tang, D., Zandbergen, H. W. & Schenk, H. (1998). *Acta Cryst.* A**54**, 91–101.

Jones, P. M., Rackham, G. M. & Steeds, J. W. (1977). *Proc. R. Soc. London Ser. A*, **354**, 197–222.

Kambe, K., Lehmpfuhl, G. & Fujimoto, F. (1974). *Z. Naturforsch. Teil A*, **29**, 1034–1044.

Lu, Z. W., Zunger, A. & Deutsch, M. (1993). *Phys. Rev. B*, **47**, 9385–9410.

Midgley, P. A., Sleight, M. E. & Vincent, R. (1996). *J. Solid State Chem.* **124**, 132–142.

Mori, N., Oikawa, T., Kato, T., Miyahara, J. & Harada, Y. (1998). *Ultramicroscopy*, **25**, 195–207.

National Bureau of Standards (1955). *Natl Bur. Stand. (US) Circ.* No. 539, Vol. 7, p. 12.

Peng, L. M., Ren, G., Dudarev, S. L. & Whelan, M. J. (1996*a*). *Acta Cryst.* A**52**, 257–276.

Peng, L. M., Ren, G., Dudarev, S. L. & Whelan, M. J. (1996*b*). *Acta Cryst.* A**52**, 456–470.

Press, W. H., Flannery, B. P., Teukolsky, J. A. & Vetterling, W. T. (1989). *Numerical Recipes.* Cambridge University Press.

Rossouw, C. J., Gibson, M. A. & Forwood, C. T. (1996). *Ultramicroscopy*, **66**, 193–209.

Saunders, M., Bird, D. M., Holbrook, O. F., Midgley, P. A. & Vincent, R. (1996). *Ultramicroscopy*, **65**, 45–52.

Saunders, M., Bird, D. M., Zaluzec, N. J., Burgess, W. G., Preston, A. R. & Humphreys, C. J. (1995). *Ultramicroscopy*, **60**, 311–323.

Spence, J. C. H. & Zuo, J. M. (1992). *Electron Microdiffraction.* New York: Plenum Press.

Stevenson, A. W., Milanko, M. & Barnea, Z. (1984). *Acta Cryst.* B**40**, 521–530.

Swaminathan, S., Altynov, S., Jones, I. P., Zaluzec, N. J., Maher, D. M. & Fraser, H. L. (1997). *Ultramicroscopy*, **69**, 169–183.

Tanaka, M. & Tsuda, K. (1990). *Proc. XIIth ICEM*, edited by L. D. Peachy & D. B. Williams, Vol. 2, pp. 518–519. San Francisco Press.

Tanaka, M. & Tsuda, K. (1991). *Proc. Microbeam Analysis*, edited by D. G. Howitt, pp. 145–146. San Francisco Press.

Tanaka, M., Tsuda, K., Terauchi, M., Tsuno, K., Kaneyama, T., Honda, T. & Ishida, M. (1998). *J. Microsc.* **194**, 219–227.
Tsuda, K. & Tanaka, M. (1995). *Acta Cryst.* A**51**, 7–19.
Tsuno, K., Kaneyama, T., Honda, T., Tsuda, K., Terauchi, M. & Tanaka, M. (1997). *J. Electron Microsc.* **46**, 357–368.
Vincent, R., Bird, D. M. & Steeds, J. W. (1984*a*). *Philos. Mag.* A**50**, 745–763.
Vincent, R., Bird, D. M. & Steeds, J. W. (1984*b*). *Philos. Mag.* A**50**, 765–786.
Weickenmeier, A. & Kohl, H. (1991). *Acta Cryst.* A**47**, 590–597.
Zuo, J. M. (1991). *Acta Cryst.* A**47**, 87–95.
Zuo, J. M., Spence, J. C. H., Downs, J. & Mayer, J. (1993). *Acta Cryst.* A**49**, 422–429.
Zuo, J. M., Spence, J. C. H. & Høier, R. (1989). *Phys. Rev. Lett.* **62**, 547–550.
Zuo, J. M. & Weickenmeier, A. L. (1995). *Ultramicroscopy*, **57**, 375–383.